FOI-R--0823--SE
March 2003
ISSN 1650-1942
Technical report

Elin Broström

Investigation of the Electromagnetic Field Distribution in an Undermoded Reverberation Chamber

Sensor Technology
SE-581 11 Linköping

SWEDISH DEFENCE RESEARCH AGENCY

Sensor Technology
P.O. Box 1165
SE-581 11 Linköping

FOI-R--0823--SE

March 2003

ISSN 1650-1942

Technical report

Elin Broström

Investigation of the Electromagnetic Field Distribution in an Undermoded Reverberation Chamber

Issuing organization
FOI – Swedish Defence Research Agency
Sensor Technology
P.O. Box 1165
SE-581 11 Linköping

Report number, ISRN
FOI-R--0823--SE

Report type
Technical report

Research area code
6. Electronic Warfare

Month year
March 2003

Project no.
E3031

Customers code
5. Commissioned Research

Sub area code
61 Electronic Warfare including Electromagnetic Weapons and Protection

Author/s (editor/s)
Elin Broström

Project manager
Mats Bäckström

Approved by
Magnus Höijer

Sponsoring agency
Swedish Armed Forces

Scientifically and technically responsible
Magnus Höijer

Report title
Investigation of the Electromagnetic Field Distribution in an Undermoded Reverberation Chamber

Abstract (not more than 200 words)

Electromagnetic radiation with high intensity can cause disturbance and destruction of electronic systems. The electromagnetic threat can be intentional, e.g. High Power Microwaves (HPM) weapons, or unintentional, e.g. radiation from radar stations. A Reverberation Chamber (RC) is a test facility that can be used to perform susceptibility tests of electronic systems.

The properties of the electromagnetic field in the chamber have to be well known to be able to use the RC. A deterministic model of the field would be very complex, and therefore field statistics are used to describe the field. Normally the RC is used for applications at high frequencies, where the chamber is over-moded, but low frequency measurements are also of great practical and economical interest. For high frequencies it exist a commonly accepted statistical model for the field in the chamber, the χ (chi) distribution.

In this Master of Science thesis some newly proposed theoretical distribution functions are compared to experimental data at low frequencies where the χ-model breaks down. The examined distributions are a Bessel K distribution, a Gamma distribution, and a so-called Compound Exponential distribution. An improvement is shown in the agreement with measured data compared to the χ-distribution function at lower frequencies.

Keywords
Reverberation Chamber, Electromagnetic field, Cumulative distribution function, Probability density function, High Power Microwaves

Further bibliographic information

Language English

ISSN 1650-1942

Pages 63 p.

Price acc. to pricelist

Utgivare	Rapportnummer, ISRN	Klassificering
Totalförsvarets Forskningsinstitut - FOI Sensorteknik Box 1165 581 11 Linköping	FOI-R--0823--SE	Teknisk rapport
	Forskningsområde 6. Telekrig	
	Månad, år Mars 2003	**Projektnummer** E3031
	Verksamhetsgren 5. Uppdragsfinansierad verksamhet	
	Delområde 61 Telekrigföring med EM-vapen och skydd	

Författare/redaktör	Projektledare
Elin Broström	Mats Bäckström
	Godkänd av Magnus Höijer
	Uppdragsgivare/kundbeteckning Försvarsmakten
	Tekniskt och/eller vetenskapligt ansvarig Magnus Höijer

Rapportens titel (i översättning)

Undersökning av fördelningsfunktioner för det elektromagnetiska fältet i en fåmodig modväxlande kammare

Sammanfattning (högst 200 ord)

Elektromagnetisk strålning med hög intensitet kan störa och till och med förstöra elektronisk utrustning. Det elektromagnetiska hotet kan vara medvetet, t.ex. högeffektpulsad mikrovågsstrålning (HPM), eller omedvetet, t.ex. strålningen från en radarstation. I en modväxlande kammare (MVK) kan elektronisk utrustning testas mot elektromagnetiska fält.

För att kunna använda kammaren krävs goda kunskaper om fältets egenskaper. Eftersom en deterministisk modell blir för komplicerad använder man statistiska modeller. Normalt används kammaren vid höga frekvenser, men det finns ett stort intresse av att kunna göra mätningar även vid lägre frekvenser. Den statistiska modell som används för höga frekvenser, χ (chi) modellen, gäller inte för låga frekvenser.

I detta examensarbete för civilingenjörsexamen jämförs tre nya förslag på fördelningsfunktioner med mätdata vid så låga frekvenser att χ-fördelningen inte gäller. De undersökta fördelningarna är en Bessel K fördelning, en Gamma fördelning och en så kallad Compound Exponential fördelning. De nya modellerna överensstämmer bättre med mätdata än χ-modellen för de undersökta frekvenserna.

Nyckelord

Modväxlande kammare, Elektromagnetiska fält, Fördelningsfunktion, Sannolikhetsfunktion, Högeffektpulsad Mikrovågsstrålning

Övriga bibliografiska uppgifter	Språk Engelska
ISSN 1650-1942	**Antal sidor:** 63 s.
Distribution enligt missiv	**Pris: Enligt prislista**

Contents

Chapter 1

Introduction

Everyone who owns a mobile telephone has probably noticed that the electromagnetic radiation can disturb other electronic equipment, e.g. a radio or television. When this happens to aircrafts, robots or medical equipments the effects can be devastating [1].

HPM, High Power Microwaves, is electromagnetic radiation with high intensity which can cause disturbance and destruction of electronic systems. HPM has become a threat against military as well as civil targets in case of war or a terrorist attack. The development of HPM sources, used as weapons, and the expansion of the electronic infrastructure e.g. telecom and power networks, has implied demands on methods for testing electronic equipments susceptibility and demands on development of shielding.

A relatively new type of test facility for doing susceptibility tests is the Reverberation Chamber (RC).

In the RC is it possible to generate large electromagnetic fields with relatively low input power, due to the RC's high Q-value[1]. To be able to make use of this benefit of the RC, the properties of the electromagnetic field in the chamber have to be well known.

Due to the complexity of the chamber its properties is not easily prescribed and a deterministic model would be very complex. Instead field statistics is used to describe the field, this is a different approach. With the field distribution function we can estimate the probability that an object is exposed to a certain field. The statistics for the maximum field levels are often of special interest.

Maxwell's equations, which are central in the theory of electromagnetics, can be combined to the well known wave equation. In free space there exists a solution to the wave equation for any frequency. In the RC, on the other hand, solutions to Maxwell's equations can only be found for a discrete number of frequencies. That is due to the boundary conditions, enforced by the walls in the reverberation chamber. These solutions are called modes.

Stirrers are used in the chamber to change the boundary conditions and the objective is to displace the modes and create a new field pattern for each stirrer position.

[1]The Q-value is the chamber's ability to store energy. See chapter 4.

The stirrers are constituted of metal blades. A change of boundaries change the frequencies for which the wave equation is solvable, the stirring displace the modes. The RC can both in design and function be compared to a microwave oven. Instead of stirrers the plate rotates in the oven to accomplish even heating.

It is not possible to achieve a homogeneous field at the individual stirrer positions, but in an ideal chamber the mean over all stirrer positions represents a homogeneous field.

Normally the RC is used for applications at high frequencies, mostly in the microwave region over 1 GHz, but low frequency measurements are also of great practical and economical interest.

At high frequencies, when the wavelength is small relative to chamber dimensions, a large number of modes are present. The chamber is said to be overmoded when the number of modes is so large that the modes overlap each other in frequency space. At lower frequencies, when the wavelength is larger relative to the chamber dimensions, only a few modes are present and the chamber is said to be undermoded.

The chamber is normally not used when it is undermoded and the limit frequency is called "the lowest usable frequency". The lowest usable frequency depend on demand for accuracy, chamber size and the stirrers ability to displace the modes. A larger chamber can be used at lower frequencies but it is more expensive to build, and due to increased losses in the walls it is not possible to achieve as high fields as in a smaller chamber. With knowledge about the field statistics at low frequencies the chamber can be used in a satisfactory way even if only a few modes are present. Hence the lowest usable frequency, or the required chamber size, can be decreased.

Chapter 2

This work

For high frequencies there exist a commonly accepted statistical model for the field in the chamber. Unfortunately in the low frequency region the assumptions fail and the model is not applicable. Proposals of distribution functions that are valid at lower frequencies was recently prepared [2].

Using a deterministic field model, i.e. describing the chamber completely and solving Maxwell's equations, is impractical due to the complexity of the stirrers, antenna and test object.[1]

In this paper some newly proposed theoretical distribution functions for undermoded chambers are compared to experimental data at so low frequencies that the model for overmoded chambers breaks down. The distributions examined are a Bessel K distribution, a Gamma distribution, and a so called Compound Exponential distribution [2]. Both the total field and the field in the three orthogonal directions are examined.

The distribution for an ideal reverberation chamber, which is used for overmoded chambers, is the χ (chi) distribution [5].

To ensure useful statistics uncorrelated samples are required. The higher number of uncorrelated samples the lower measurement uncertainty can be achieved. Actually the samples have to be independent but investigations have shown that in this case uncorrelated and independent are equivalent [6]. Using large and independently rotating stirrers increase the number of uncorrelated stirrer positions and thus the number of uncorrelated samples [6].

At low frequency measurements, when the modes are few and the stirring process does not manage to displace the modes enough, a larger number of stirrer positions become correlated. This is taken into account when the number of stirrer positions is chosen.

At certain frequencies the models seem to break down. A large discrepancy be-

[1] In principal a numerical approach as e.g. FDTD [3] may be used. This has also been done, e.g. [4]. However, the large volume of the RC compared to the wavelength of the electromagnetic field, implies very large memory requirements of the computer system, and is in practice only durable for very low frequencies [4].

tween measured data and the data predicted by the theoretical distribution were observed. An attempt to explain this is made.

The work, which has been submitted to the School of Engineering Physics, Royal Institute of Technology, Stockholm, in partial fulfillment of the requirements for the degree of Master of Science, has been performed at the Department of Microwave Technology, Swedish Defence Research Agency, FOI, Linköping.

Chapter 3

Electromagnetic field and waves

A field is a distribution of a quantity, which may be independent of time. Waves are time and space dependent fields.

Electric fields are associated with charges. When the charge vary with time the electric field is accompanied by a magnetic field. Time-varying electric and magnetic fields are coupled and give rise to an electromagnetic field. Electromagnetic fields can produce electromagnetic waves that convey energy. The electromagnetic waves propagate with the speed of light.

There are four fundamental field quantities in electromagnetics, electric field intensity ($\overline{E}$), electric flux density ($\overline{D}$), magnetic flux density ($\overline{B}$), and magnetic field intensity, ($\overline{H}$).

The power density of an electromagnetic field, which is known as the *Poynting's vector* is defined by

$$\overline{S} = \overline{E} \times \overline{H}. \tag{3.1}$$

Poynting's vector represents the power flow per unit area (W/m^2) and is orthogonal to both $\overline{E}$ (V/m) and $\overline{H}$ (A/m).

Material or medium properties determine the relations between E and D and between H and B. The relation between E and H is

$$E = \eta H \tag{3.2}$$

where η is the intrinsic impedance [7].

Maxwell's equations are summarized as follows.

$$\nabla \times \overline{E} = -\frac{\partial \overline{B}}{\partial t} \tag{3.3}$$

$$\nabla \times \overline{H} = \overline{J} - \frac{\partial \overline{D}}{\partial t} \tag{3.4}$$

$$\nabla \cdot \overline{D} = \rho \tag{3.5}$$

$$\nabla \cdot \overline{B} = 0, \tag{3.6}$$

where $\overline{J}$ is the density of free currents and ρ is the volume density of free charges [7]. An electromagnetic field can be written $E_\alpha + iE_\beta$. E_α is the so-called *in-phase component* and E_β is the so called *quadrature component*. The phase differs 90 degrees between the quadrature and in-phase components.

3.1 Phasor notation

When dealing with electromagnetic waves it is convenient to use *phasor notation*. To specify a sinusoidal quantity knowledge of three parameters, amplitude, phase and frequency is required. The time-dependent expression of a sinusoidal quantity can be written as either a sine or a cosine function. If a cosine function is chosen as the reference, then all derived results refer to the cosine function. It is inconvenient to work directly with the cosine function because differentiation and integration lead to both cosine and sine functions which is tedious to combine.

The phasor notation involve exponential functions, these functions are called *phasors* and contain amplitude and phase information but are independent of time. The phasors are complex. The time-variable expression is given by the real part of the product of the phasor and $e^{i\omega t}$, if the reference function is a cosine function and by the imaginary part if the reference is a sine function.

3.2 Modes and plane waves

A uniform plane wave is a particular solution of Maxwell's equations. It has a phase as well as an amplitude and therefore it is convenient to use phasor notation. Maxwell's equations can be combined to yield wave equations that predict the existence of electromagnetic waves. A mode is a solution to the electromagnetic wave equation with boundary conditions. In the wave equation below c is the speed of light,

$$\nabla^2\overline{E} - \frac{1}{c^2}\frac{\partial^2\overline{E}}{\partial t^2} = 0. \tag{3.7}$$

The number of modes in a chamber with volume V is approximately (see [5])

$$N \approx \frac{V}{\lambda^3}, \tag{3.8}$$

where λ is the wavelength. The relation between frequency and wavelength is $f = \frac{c}{\lambda}$.

When the wavelength increases it becomes more difficult to find solutions to the wave equation with boundary conditions. Therefore the mode density decreases with wavelength, or equivalently stated, increases with frequency.

The width of a mode can be calculated from an application of the Q-value

$$Q = \frac{\omega}{\triangle\omega}, \tag{3.9}$$

where $\triangle\omega$ is the mode width.

3.3 Eigenfrequencies

Cavities such as the reverberation chamber have resonance frequencies, or eigenfrequencies. The eigenfrequencies in an empty chamber are given by

$$f_{nmp} = \frac{c}{2}\sqrt{\left(\frac{m}{a}\right)^2 + \left(\frac{n}{b}\right)^2 + \left(\frac{p}{d}\right)^2}, \tag{3.10}$$

where m, n and p are integers, at least two of them shall differ from zero, a, b and d are the dimensions of the chamber. There is an eigenfrequency associated to every mode. Principally there is no solution to Maxwell's equations for other frequencies, but due to the metal in the walls has a finite conductivity a range of frequencies made up the mode width according to (3.10). For $a \leq b \leq d$, the lowest eigenfrequency is given by f_{011} [7]. The resonance frequencies lie closer at higher frequencies.

Chapter 4

The Reverberation Chamber

The reverberation chamber is a rectangular room with conducting metal walls, see figure A.41.

Power is transmitted into the chamber by an antenna. To be able to transmit power, the antenna needs to find a receiving mode, otherwise the power is reflected back to the source.

In addition to the problem with correlated stirrer positions the antenna has problem transmitting energy into the chamber at low frequencies due to the limited number of modes. Radiation is either absorbed or reflected.

There are energy losses in the chamber due to absorption in the walls and stirrers, as well as in antennas and test equipment placed in the chamber, and due to leakage by the door and through holes for cables. The higher conductivity of the walls the less losses. The energy losses are specified by the Q-value that is defined as ω times the quotient between the energy (W) in the chamber and the energy ($P_{input}T$) transmitted into the chamber during one period (T), ω is 2π times the frequency f

$$Q \triangleq \frac{\omega W_{inside}}{P_{input}} = \frac{2\pi f W_{inside}}{P_{input}} = \frac{2\pi W_{inside}}{P_{input}T}. \tag{4.1}$$

The Q-value is a useful quantity because it allows prediction of the field strength from the input power.

Every electromagnetic wave is reflected repeatedly by all reflective areas and a standing wave pattern is created. It is desirable to have high mode density to be assured of that the test object is illuminated from different directions and to decrease the probability of, for every stirrer position, getting a field minimum where the object is placed.

In an ideal chamber, the field at the different stirrer positions are statistically independent from each others and the field vary randomly with stirrer position. The field at a given stirrer position and location is the sum of all phasors of the contributing modes. The excitation of the modes is independent and random. One way to imagine the situation is to assume waves originating from different boundary segments, so called "facets". The facets are considered randomly positioned and oriented [2]. In

addition to testing devices durability under irradiation of HPM the RC is used for electromagnetic compatibility (EMC) testing, e.g. emission measurements and measuring antenna efficiency. EMC is electronic devices ability to operate compatibly with other electronic devices.

If the stirring is made in discrete steps the chamber is called a Mode-Tuned Reverberation Chamber, if the stirring is continuous it is called a Mode Stirred RC. There is a discrepancy in the terminology of reverberation chambers, sometimes the name Mode-Stirred Reverberation Chamber is used with the same meaning as Reverberation Chamber. This is of course very confusing and therefore the word Reverberation Chamber is used consistently to denote the actual chamber in this paper.

4.1 The Anechoic Chamber

An alternative test facility with the same applications as a RC is the anechoic chamber (AC). An AC is a large room in which the interior surfaces are covered with absorbing material.

In an ideal anechoic chamber there is no reflection in the boundaries and free space conditions are fulfilled.

Measurements in reverberation chambers and anechoic chambers are comparable, the mean over all stirrer positions in the RC corresponding to the mean over all directions in the AC.[1]

In ACs are all parameters deterministic. A drawback with ACs compared to RCs is that a careful measurement require that the test object is irradiated from all directions which takes much time. An advantage is that it is possible to decide in which direction the test object is most sensitive to radiation.

[1] See C.

Chapter 5

Stirring and correlation

It is desirable to have many samples to achieve good estimations for mean and variance. It is not clear yet what happens when data are correlated, however correlated samples does not provide more information. Is uncorrelated samples a uncompromisable demand or is it not necessary for being able to consider the result? That question is stilled to be answered, but is not addressed here.

5.1 Correlation coefficient

Correlation is defined as a correlation coefficient being larger than a certain value, chosen with respect to desired confidence level.

The linear correlation coefficient, ρ, is calculated as [12],

$$\rho(r) = \frac{1}{N-1} \frac{\sum_{i=1}^{N} (E_{x_i} - \langle E_x \rangle)(E_{x_{i+r}} - \langle E_x \rangle)}{\sigma_x^2}, \tag{5.1}$$

where N is the number of stirrer positions, E_{x_i} is the field at stirrer position i and $E_{x_{i+r}}$ is the field at position i+r. If $r = 1$ it is one step between consecutive stirrer positions. $\langle E_x \rangle$ is the mean of the field over all stirrer positions.

5.2 Stirrer efficiency

An investigation of stirrer efficiency, i.e. how the stirring affects the number of uncorrelated samples, has been made in the FOI Mode Tuned Reverberation Chamber [12]. The intention was to decrease the lowest usable frequency limit by managing to displace modes more with a more effective stirring. Stirrers of different size were used.

It was shown that increasing the stirrer area results in more effective stirring, i.e. displacement of modes. The best result were accomplished when two large stirrers are used simultaneously, one rotating horizontally and one rotating vertically [12]. A later work on this subject show that rotating the two stirrers independently gives even

more uncorrelated samples [6]. Therefore the set-up with two large, independently rotating stirrers is used during all measurements in this work.

It was also shown that the correlation between the different stirrer positions decrease with frequency. This is explained by the fact that a change of boundary conditions manage to change the field pattern more when the number of modes is larger.

5.3 Uncorrelation gives independence

Statistical independence implies uncorrelation but the opposite statement is not true in general [8]. The relation between statistical independence and uncorrelation of measured data has been examined [6]. This to be assured of that the assumption that uncorrelated values are statistically independent are acceptable. The assumption is doubtful in the cases when only one stirrer is used but when two stirrers are stepped independently the assumption can be used without loss of generality [6].

Why not use an independent coefficient instead of using a correlation coefficient? The correlation coefficient is much simpler to calculate and even if statistical independence is not proved, this is a way to reject data which are dependent.

Chapter 6

Theoretical model for the field in overmoded chambers

6.1 Distribution function

The cumulative distribution function for the random variable X is defined as

$$F_X(x) = P(X \leq x),\ -\infty < x < \infty, \tag{6.1}$$

where $P(X \leq x)$ is the probability that $X \leq x$.

The probability density function ($f_X(x)$) for continuous distributions has the property [11]

$$F_X(x) = \int_{-\infty}^{x} f_X(y)dy,\ -\infty < x < \infty. \tag{6.2}$$

A cumulative distribution function (cdf) has values in the interval [0,1] and is cumulative.

A probability density function (pdf) for a sample of measurement data can be illustrated with a histogram, see figure A.5. The value at 4600 V/m are examples of the so-called outliers.

One of the main advantages of having a pdf or a cdf for the field in the chamber is that estimates, e.g. for the mean and variance and their accuracies, can be calculated.

6.2 The χ distribution

This analysis is presented in [5] and it is based on that a large number of modes are present in the chamber. Since the field has quadrature and in-phase components in each of the three orthogonal directions, six parameters are required for every frequency to describe the field at a point. The mean of each quadrature component is assumed to be zero and the variance is σ^2.

Assuming that the contributions from the large number of modes to the amplitude at a point being random, independent and identically distributed implies that each of the six parameters is a sum of a large number of independent, identically distributed random variables and hence they should be normally distributed by the central limit theorem. If the measurement point is near any wall the assumption of independence is weaker since the field always is zero by the walls.

The magnitude of the total power density, S_{tot}, is the sum of the power density in all three directions,

$$S_{tot} = S_x + S_y + S_z. \tag{6.3}$$

E being proportional to H (see equation (3.1) and (3.2)) gives that the power density is proportional to the square of the field,

$$S \propto E^2. \tag{6.4}$$

Hence

$$|E_{tot}|^2 = |E_x|^2 + |E_y|^2 + |E_z|^2 . \tag{6.5}$$

The real (Re) and imaginary (Im) part of E_n represent the quadrature and in-phase components,

$$|E_n|^2 = (Re\{E_n\})^2 + (Im\{E_n\})^2 \text{ where } n = x, y, z. \tag{6.6}$$

The magnitude of the total field is thus the square root of the sum of the squares of six normally distributed random variables,

$$|E_{tot}| = \sqrt{(Re\{E_x\})^2 + (Im\{E_x\})^2 + (Re\{E_y\})^2 + (Im\{E_y\})^2 + (Re\{E_z\})^2 + (Im\{E_z\})^2}. \tag{6.7}$$

In the following theorem is $N(m, \sigma)$ the normal distribution.

Theorem 1 *[8] Let X_i, $i = 1 \ldots, n$, be independent random variables and $X_i \in N(m, \sigma)$. Then $\frac{1}{\sigma^2}\sum_{i=1}^{n}(X_i - m)^2 \in \chi^2(n)$*

According to theorem (1) is $\frac{E_n^2}{\sigma^2}$ χ^2 distributed with two degrees of freedom.

Theorem 2 (Property of χ^2 distribution) *[8] If X and Y are independent and $X \in \chi^2(f_1)$, $Y \in \chi^2(f_2)$. Then $X + Y \in \chi^2(f_1 + f_2)$.*

Theorem (2) with equation (6.5) gives that $\frac{E_{tot}^2}{\sigma^2}$ is χ^2 distributed with six degrees of freedom.

Put $Y = \frac{E_{tot}}{\sigma}$ and $X = \frac{E_{tot}^2}{\sigma^2}$, then $Y = \sqrt{X}$. The distribution function $F_Y(y)$ equals the distribution function $F_X(y^2)$, derivation gives the probability density function $f_Y(y) = 2yf_X(y^2)$. Hence

$$f_{(\frac{E_{tot}}{\sigma})}(\frac{e_{tot}}{\sigma}) = 2\frac{e_{tot}}{\sigma} f_{(\frac{E_{tot}^2}{\sigma^2})}(\frac{e_{tot}^2}{\sigma^2}). \tag{6.8}$$

Since $f_{(\frac{E_{tot}^2}{\sigma^2})}(\frac{e_{tot}^2}{\sigma^2}) \in \chi^2(6)$ the probability density function for the total field is given by

$$f_{(\frac{E_{tot}}{\sigma})}(\frac{e_{tot}}{\sigma}) = \frac{2^{1-n/2}}{\Gamma(\frac{n}{2})}(\frac{e_{tot}}{\sigma})^{n-1} e^{-\frac{e_{tot}^2}{2\sigma^2}}, \tag{6.9}$$

where n is the degree of freedom, which is two times the dimension. For the total field is the degree of freedom 6 since the dimension is 3. The variable e_{tot} is used to separate it from the random variable E_{tot}. Comparing (6.9) to the definition of the χdistribution with six degrees of freedom show that $\frac{E_{tot}}{\sigma} \in \chi(6)$ and hence $E_{tot} \in \chi(6)$. The final pdf for E_{tot} becomes

$$f_{E_{tot}}(e_{tot}) = \frac{e_{tot}^5 e^{\frac{-e_{tot}^2}{2\sigma^2}}}{8\sigma^6}. \tag{6.10}$$

Integration from 0 to e_{tot} gives the distribution function.

$$F_{E_{tot}}(e_{tot}) = 1 - \frac{1}{2} e^{-\frac{e_{tot}^4}{2\sigma^2}} (\frac{e_{tot}^4}{4\sigma^2} + \frac{e_{tot}^2}{\sigma} + 2). \tag{6.11}$$

The probability density function for E_n is achieved in the same way, now with $n = 2$,

$$f_{E_n}(e_n) = \frac{e_n}{\sigma^2} e^{\frac{-e_n^2}{2\sigma^2}}. \tag{6.12}$$

And the distribution function

$$F_{E_n}(e_n) = 1 - e^{\frac{-e_n^2}{2\sigma^2}}. \tag{6.13}$$

Investigations show that these statistics serve as a good model for the fields in an overmoded chamber [5]. This model is based on the assumption that a large number of modes are present, naturally it is not applicable for undermoded chambers.

6.2.1 Estimation of σ^2

The maximum-likelihood method of estimating distribution parameters is used to estimate σ^2. The *likelihood function* L for $\hat{\sigma}^2$ is defined as

$$L(\hat{\sigma}^2) = f(E_1, \hat{\sigma}^2) * f(E_2, \hat{\sigma}^2) \ldots f(E_n, \hat{\sigma}^2), \tag{6.14}$$

where $\hat{\sigma^2}$ is the maximum-likelihood estimate for σ^2. Maximizing L is the same as maximizing the logarithm of L. Differentiation of ln L with respect to σ^2 and setting it equal to zero yields

$$\hat{\sigma}^2 = \frac{1}{6m}\sum_{i=1}^{m} E_i^2 \triangleq \frac{\overline{E^2}}{6}, \tag{6.15}$$

for the pdf with six degrees of freedom and

$$\hat{\sigma}^2 = \frac{1}{2m}\sum_{i=1}^{m} E_i^2 \triangleq \frac{\overline{E^2}}{2}, \tag{6.16}$$

for the pdf with two degrees of freedom, m is the number of data samples. Thus the estimator is the average of the square of the E-field divided by the number of degrees of freedom.

Chapter 7

Proposals for field statistics in undermoded chambers

7.1 The Bessel K distribution

For an arbitrary position and stirrer position the chamber's walls and stirrers can be replaced by independently scattering surfaces, or facets. The number of facets depends on stirrer position. Averaging across a sufficiently large number of independent stirrer positions, the ensemble power density can be assumed to be approximately equally distributed across all facets [2].

Because of the complexity of the analysis that leads to the result used here, only the final probability and distribution functions for the field are presented. The derivations can be found in [2].

Below $K_n(x)$ is the modified Bessel function of the second kind of order n, and $\Gamma(x)$ is the Gamma function.

The Bessel K distribution functions includes the distribution parameters, M and b, which can be estimated as follows

$$M_n = \frac{2\mu_{S_n}^2}{\sigma_{S_n}^2 - \mu_{S_n}^2}, \tag{7.1}$$

$$b_n = \sqrt{\frac{8\mu_{S_n}}{\sigma_{S_n}^2 - \mu_{S_n}^2}}, \tag{7.2}$$

$$M_{tot} = \frac{4\mu_{S_{tot}}^2}{3\sigma_{S_{tot}}^2 - \mu_{S_{tot}}^2}, \tag{7.3}$$

$$b_{tot} = \sqrt{\frac{48\mu_{S_{tot}}}{3\sigma_{S_{tot}}^2 - \mu_{S_{tot}}^2}}, \tag{7.4}$$

where μ_S is the mean and σ_S is the standard deviation of the ensemble. The distribution parameters are positive and M can be thought of as a parameter proportional

to the number of modes in the chamber.[1] The probability function of E_n becomes

$$f_{E_n}(e_n) = \frac{b_n^{M_n+1}}{2^{M_n-1}\Gamma(M_n)} e_n^{M_n} K_{M_n-1}(b_n e_n). \tag{7.5}$$

Integration gives the distribution function

$$F_{E_n}(e_n) = 1 - \frac{(b_n e_n)^{M_n} K_{M_n}(b_n e_n)}{2^{M_n-1}\Gamma(M_n)}, \tag{7.6}$$

and the probability function of E_{tot} is

$$f_{E_{tot}}(e_{tot}) = \frac{b_{tot}^{M_{tot}+3}}{2^{M_{tot}+2}\Gamma(M_{tot})} e_{tot}^{M_{tot}+2} K_{M_{tot}-3}(b_{tot} e_{tot}). \tag{7.7}$$

The distribution function is achieved by integration from 0 to e_{tot}. This is not done explicitly, instead a numerical solution performed by Matlab is used.

It can be shown that the Bessel K distribution converges towards the χ distribution when M goes to infinity.

7.2 The Gamma distribution

Another attempt to describe the field in undermoded chambers theoretically is the Gamma distribution. The theory is also based on contributions to the field from facets. Different forms of functions for the power that result in different probability density functions are examined. A function that gives a result that agree well with experimental data is chosen [2].

The probability density function then becomes

$$f_{|E|}(|e|) = \frac{2\mathcal{M}^{\frac{\mathcal{M}(1-\eta)}{2}}(1-\eta)}{\Gamma(\mathcal{M})\sigma_{\chi^2_{2p\mathcal{M}}}^{\mathcal{M}(1-\eta)}} |e|^{2\mathcal{M}(1-\eta)-1} \, exp\left[-\left(\frac{\sqrt{\mathcal{M}}\,|e|^2}{\sigma_{\chi^2_{2p\mathcal{M}}}}\right)^{1-\eta}\right], \tag{7.8}$$

where $\sigma_{\chi^2_{2p\mathcal{M}}} = 2\sqrt{p\mathcal{M}}$; this is the standard deviation for a χ^2-distribution with $2p\mathcal{M}$ degrees of freedom. Solving the non-linear equation system below gives estimators for $\mathcal{M}$ and η,

$$\mu_S = \frac{\sigma_{\chi^2_{2p\mathcal{M}}}}{\sqrt{\mathcal{M}}} \frac{\Gamma[\mathcal{M} + (1-\eta)^{-1}]}{\Gamma(\mathcal{M})}, \tag{7.9}$$

$$\sigma_S^2 = \frac{\sigma^2_{\chi^2_{2p\mathcal{M}}}}{\mathcal{M}} \frac{\Gamma[\mathcal{M} + 2(1-\eta)^{-1}]}{\Gamma(\mathcal{M})} - \mu_S^2. \tag{7.10}$$

The mean μ_s and the variance σ_s^2 of the power density are given from measurement. Since the non-linear system is difficult to solve, η and $\mathcal{M}$ are not calculated in this paper.

[1] More specific; p times the number of plane waves constituting the electromagnetic field in the chamber. The factor p is 1 for M_n and 3 for M_{tot}.

7.3 The Compound Exponential distribution

The analysis, that leads to a Compound Exponential distribution function, is based on decomposition of the partially polarized field into one completely polarized component and one non-polarized component. In an ideal chamber only the unpolarized component exists [9].

A polarization matrix $\overline{\overline{J}}$, is defined as

$$\overline{\overline{J}} = \begin{pmatrix} \langle E_x E_x^* \rangle & \langle E_x E_y^* \rangle & \langle E_x E_z^* \rangle \\ \langle E_y E_x^* \rangle & \langle E_y E_y^* \rangle & \langle E_y E_z^* \rangle \\ \langle E_z E_x^* \rangle & \langle E_z E_y^* \rangle & \langle E_z E_z^* \rangle \end{pmatrix}, \tag{7.11}$$

where $*$ denotes the conjugate and $\langle \cdot \rangle$ averaging over all stirrer positions.

The polarization matrix is Hermitian, i.e. $\overline{\overline{J}} = \overline{\overline{J^*}}$. The conjugate transpose $\overline{\overline{J^*}}$ is obtained by interchanging the rows and columns and taking the complex conjugate of each entry. Hermitian matrixes are diagonalizable [10].

Diagonalization of $\overline{\overline{J}}$ eliminate the off-diagonal element, which often are unknown since they are difficult to measure. The eigenvalues, that will appear on the diagonal after the diagnalization, are denoted λ_x, λ_y and λ_z. They are real and positive because every eigenvalue of a Hermitian matrix is real [10].

The resulting diagonal matrix $\overline{\overline{\Lambda}}$ can be written

$$\overline{\overline{\Lambda}} = \begin{pmatrix} \lambda_x & 0 & 0 \\ 0 & \lambda_y & 0 \\ 0 & 0 & \lambda_z \end{pmatrix} = \begin{pmatrix} \lambda_z & 0 & 0 \\ 0 & \lambda_z & 0 \\ 0 & 0 & \lambda_z \end{pmatrix} + \begin{pmatrix} \lambda_x - \lambda_z & 0 & 0 \\ 0 & 0 & 0 \\ 0 & 0 & 0 \end{pmatrix} + \begin{pmatrix} 0 & 0 & 0 \\ 0 & \lambda_y - \lambda_z & 0 \\ 0 & 0 & 0 \end{pmatrix} \tag{7.12}$$

In equation (7.12), the first term of the sum corresponds to the non-polarized part of the field. The remaining two terms correspond to the polarized part of the field. Here λ_z is chosen to be a reference value for the unpolarized field. This choice is arbitrary and leads to a pdf which is asymmetric with respect to its distribution parameters. The distribution function is called Asymmetric Compound Exponential Distribution Function (ACE).

Symmetric forms of compound exponential distributions functions (SCE) can also be derived, they give the same final distribution function as the asymmetric form. The asymmetric form is used here because it only requires two distribution parameters, the symmetric form needs three [9].

The elements on the diagonal of $\overline{\overline{J}}$ can be achieved by measuring E_n,

$$\langle E_n E_n^* \rangle = \langle E_n^2 \rangle . \tag{7.13}$$

The total power density S_{tot} equals the sum of the diagonal of $\overline{\overline{J}}$, i.e the trace of $\overline{\overline{J}}$,

$$S_{tot} = \langle E_x^2 \rangle + \langle E_y^2 \rangle + \langle E_z^2 \rangle. \tag{7.14}$$

The trace of a matrix is invariant under a change of base and thus

$$S_{tot} = tr\overline{\overline{J}} \equiv tr\overline{\overline{\Lambda}} \triangleq \lambda_x + \lambda_y + \lambda_z. \tag{7.15}$$

The distribution parameters are denoted by P_{13} and P_{23} and are defined as

$$P_{13} \triangleq \frac{\lambda_x - \lambda_z}{\lambda_x + \lambda_y + \lambda_z}, \tag{7.16}$$

$$P_{23} \triangleq \frac{\lambda_y - \lambda_z}{\lambda_x + \lambda_y + \lambda_z}. \tag{7.17}$$

Estimating the eigenvalues of $\overline{\overline{J}}$ expressed in S_n and assuming that they are normally distributed, gives the probability density functions for the magnitude of the Cartesian components of the power density,

$$f_{S_n}(s_n) = \alpha_n e^{-\alpha_n s_n}. \tag{7.18}$$

The characteristic function of the total power density is the product of the characteristic functions of the Cartesian components [11]. Inverse Fourier transform of the characteristic function of S_{tot} gives the probability density function [9]

$$f_{S_{tot}}(s_{tot}) = \sum_{x,y,z} \frac{\beta_n}{\alpha_n} e^{-\alpha_n s_{tot}}, \tag{7.19}$$

where

$$\alpha_x \triangleq \frac{3}{trJ(1 + 2P_{13} - P_{23})}, \tag{7.20}$$

$$\beta_x \triangleq \frac{1}{tr^2 J P_{13}(P_{13} - P_{23})}, \tag{7.21}$$

$$\alpha_y \triangleq \frac{3}{trJ(1 + 2P_{23} - P_{13})}, \tag{7.22}$$

$$\beta_y \triangleq \frac{1}{tr^2 J P_{23}(P_{23} - P_{13})}, \tag{7.23}$$

$$\alpha_z \triangleq \frac{3}{trJ(1 - P_{13} - P_{23})}, \tag{7.24}$$

$$\beta_z \triangleq \frac{1}{(tr^2 J P_{13} P_{23})}. \tag{7.25}$$

and *tr* denotes the trace. Because the total power density is proportional to the square of the field we have $f_E(E) = f_S(E^2)2E$. The pdf for E_n thus becomes

$$f_{|E_n|}(|e_n|) = 2e_n\alpha_n e^{-\alpha_n e_n^2} \tag{7.26}$$

and the pdf for the total field

$$f_{E_{tot}}(E_{tot}) = \sum_{n=1}^{3} \frac{2E_{tot}\beta_n}{\alpha_n} e^{-\alpha_n E_{tot}^2}. \tag{7.27}$$

Integration of (7.26) and (7.27) from 0 to e_n and e_{tot} respectively, gives the distribution functions,

$$F_{E_n}(e_n) = 1 - e^{-\alpha_n e_n^2}, \tag{7.28}$$

and

$$F_{E_{tot}}(e_{tot}) = \sum_{n=1}^{3} \frac{\beta_n}{\alpha_n^2}(1 - e^{-\alpha_n e_{tot}^2}). \tag{7.29}$$

7.3.1 Estimation of distribution parameters

Because the off-diagonal elements are unknown, approximations for P_{13} and P_{23} are needed. Two different approximations are suggested in [9].

Substituting $\langle E_n^2 \rangle$ for λ_n in (7.16) gives the first approximation.

$$P'_{13} = \frac{\langle E_x^2 \rangle - \langle E_z^2 \rangle}{\langle E_x^2 \rangle + \langle E_y^2 \rangle + \langle E_z^2 \rangle}, \tag{7.30}$$

$$P'_{23} = \frac{\langle E_y^2 \rangle - \langle E_z^2 \rangle}{\langle E_x^2 \rangle + \langle E_y^2 \rangle + \langle E_z^2 \rangle}. \tag{7.31}$$

The accuracy of these estimates increases as $\lambda_n \to \langle E_n^2 \rangle$, i.e. as the off-diagonal elements $\langle E_\alpha E_\beta^* \rangle \to 0$, this is true when the components are uncorrelated, which in turn is true for higher frequencies.

Actually the ACE distribution function with this approximation is the same as the χ distribution function for the component fields, E_x, E_y and E_z.

Recall the χ distribution function for E_n,

$$F_{E_n}(e_n) = 1 - e^{\frac{-e_n^2}{2\sigma^2}}. \tag{7.32}$$

The maximum likelihood estimate for σ^2 equals $\frac{\langle E_n^2 \rangle}{2}$, see (6.16), which gives

$$F_{E_n}(e_n) = 1 - e^{\frac{-e_n^2}{\langle E_n^2 \rangle}}. \tag{7.33}$$

Obviously α_n equals $\frac{1}{\langle E_n^2 \rangle}$ when using the first approximation. This in conjugation with equation (7.28) gives an ACE distribution function for E_n that equals (7.33).

The second approximation is not as obvious as the first one,

$$P'_{13} = \frac{\langle E_y^2 \rangle (\langle E_z^2 \rangle - \langle E_x^2 \rangle)}{\langle E_x^2 \rangle \langle E_y^2 \rangle + \langle E_x^2 \rangle \langle E_z^2 \rangle + \langle E_y^2 \rangle \langle E_z^2 \rangle}, \tag{7.34}$$

$$P'_{23} = \frac{\langle E_x^2 \rangle (\langle E_z^2 \rangle - \langle E_y^2 \rangle)}{\langle E_x^2 \rangle \langle E_y^2 \rangle + \langle E_x^2 \rangle \langle E_z^2 \rangle + \langle E_y^2 \rangle \langle E_z^2 \rangle}. \tag{7.35}$$

In the derivation of this approximation $\langle E_n^2 \rangle$ is again substituted for λ_n but now it is also assumed that $\lambda_x \to 0$ and $\lambda_y \to 0$.

The result that we will use from this analysis is (7.28) and (7.29) with the two different approximations for α_n and β_n.

Chapter 8

Measurements

8.1 Measurement set-up

The measurements were performed in one of FOI's RCs, denoted E3. The chamber size is $5.10 \times 2.46 \times 3.0$ m and, with help of equation (3.10), the lowest resonance frequency is calculated to 58 MHz. However, measurements have shown resonance frequencies lower than 58 MHz [12]. One explanation of this discrepancy is the limited conductivity of the walls, but this effect is to small to fully explain the discrepancy. Instead the main reason is probably the stirrers, which act as nodes (zeros) for the electromagnetic field, recall that equation (3.10) holds for the empty chamber. The measurement set-up is shown in figure A.44. For more details about the chamber and stirrers see [12].

The two stirrers rotate in discrete steps, independently of each other. They are made up by folded metal blades.

We used a SA-log periodic antenna, to excite the chamber. This type of antenna was chosen because it works for the frequencies (100 MHZ up to 1 GHz) that we are interested of.

To measure the field in the RC we used an E-field probe. The E-field probe measures the amplitude of the electromagnetic field in three orthogonal directions at its position. A picture of the probe, see figure A.43

The transmitting antenna is pointed into a corner to avoid direct coupling with the probe, which functions as a receiving antenna. The antenna and probe were placed on Styrofoam.

To get sufficient high input power a power-amplifier is used. The amplifier is of AR-type, to the left in figure A.42.

The power meter, in the middle of figure A.42, is used for measuring the transmitted and reflected energy.

Only a part of the transmitted and reflected power is measured, this percentage is given by the parameters of a directional coupler. The measurement is performed from the PC and all data are stored here.

8.2 S-parameters

S-parameters are used to calculate reflection in antennas and transitions.

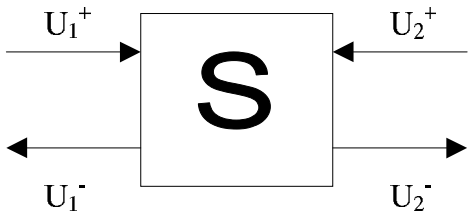

$$S_{11} = \frac{U_1^-}{U_1^+}|_{U_2^+=0}, \tag{8.1}$$

$$S_{21} = \frac{U_2^-}{U_1^+}|_{U_2^+=0}, \tag{8.2}$$

$$S_{22} = \frac{U_2^-}{U_2^+}|_{U_1^+=0}, \tag{8.3}$$

$$S_{12} = \frac{U_1^-}{U_2^+}|_{U_1^+=0}, \tag{8.4}$$

$$\tag{8.5}$$

Here S_{11} and S_{22} are reflection coefficients. If the component is reciproc S_{12} and S_{21} are identical. Most components are reciproc.

8.3 Directional coupler and power meter

The directional coupler has four gates, denoted 1 to 4. $S_{21}^{4\to2}$ denotes S_{21} for the transition from gate 4 to gate 2.

It is important that transmitted energy into the chamber is kept at a constant level because the electric field intensity increases with the transmitted power into the chamber. We have to compensate for the decrease of transmitted power for lower frequencies. We have to compensate for the fact that a different amount of energy is transmitted into the chamber for different frequencies. The directional coupler takes out a given percentage of the power, measured by the power meter. The power transmitted and reflected, can then be calculated.

The transmitted power is denoted P_3 and the reflected power is denoted P_4. See figure A.1 for P_3 and P_4 at 340 MHz. The power transmitted into the chamber is approximately $P_3/(S_{21}^{1\to3})^2$ and the total reflected power $P_4/(S_{12}^{4\to2})^2$. See figure 8.1.

The parameters of the directional coupler are specified by its manual. To get more precise values the directional coupler's S-parameters were also measured by a network

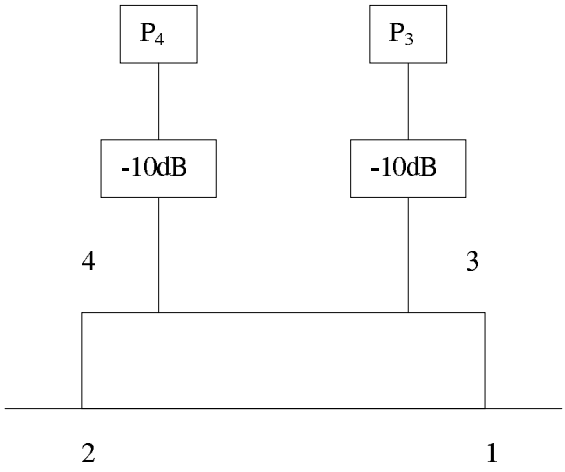

Figure 8.1: Schematic figure of the directional coupler and dampers.

analyzer, which is a careful instrument. The network analyzer was calibrated before the measurement.

Dampers (-10 dB[1]) were used to restrict the power into the power meter, these were included in the network analyzer measurement of the directional coupler. Losses in cables and transitions were neglected.

A compensation coefficient, denoted by k, has been calculated for each stirrer position and frequency to compensate for the difference in transmission and reflection for different stirrer positions and different frequencies,

$$k = \sqrt{\frac{1}{1 - \frac{P_4/(S_{12}^{4\to 2})^2}{P_3/(S_{21}^{1\to 3})^2}}}. \tag{8.6}$$

We take the square root because P_3 and P_4 is the transmitted and reflected power and we want to compensate for differences in field intensity. The field is multiplied with a different coefficients for different stirrer positions and different frequencies. An increase of the power 9 times results in an increase of the field intensity 3 times. If there is no reflection the coefficient becomes one. Sometimes the reflection is larger than the transmission, this gives a complex coefficient. In these cases the reflection is set to 99 %, which gives k=10. It is physically impossible to get larger reflection than transmission, the phenomena depend on measuring error or that $P_4/(S_{12}^{4\to 2})^2$ and $P_3/(S_{21}^{1\to 3})^2$ are approximations. A reflection of 50% of the power gives k=$\sqrt{2}$.

8.4 Electric field measurement

After the preparations described above it is time to measure the field.

[1]See B.1.

During a measurement the chosen frequencies are stepped and P_3, P_4, E_x, E_y, E_z and E_{tot} are stored for each frequency. The stirrers are moved and a new set of samples is stored.

Frequencies between 45 MHz and 1 GHz were measured for 25×25 stirrer positions. All measured frequencies are listed in table A.2.

Due to limitations of the E-field probe's battery, the maximum number of frequencies, in each measurement, is 50. To decrease the measurement time, the fastest power meter available was used. A measurement of 50 frequencies and 625 stirrer positions takes about ten hours. The input power is 15 dBm[2].

A problem is that results from different set of measurements cannot be compared because they differ for the same frequency. The explanation is that the field vary with position and the probe is moved from its position to be loaded between each measurement, furthermore the stirrers' start position is changed from one measurement to another.Temperature differences also causes different stress on the walls and thereby also changing the boundaries of the chamber.

An attempt to examine this variation was made by measuring the same frequency time after time. The problem was that the stirrer positions are changed before the frequency, therefore the conditions differ from those when the same frequency is measured in different sets. The mean and maximum E-field for 100-600 MHz is plotted in figure A.2. The peak at 570 MHz is a so-called outlier.

8.4.1 Noise measurement

A measurement of the background noise in the chamber was performed. It showed that the noise stayed at a constant level, about 0.9 V/m. This is much smaller than the electric field intensities that were measured when we used the amplifier, with an input of 15 dBm. Hence the influence of noise is neglected. Maximum noise E-field for frequencies 45-1000 MHz is shown in figure A.3.

8.5 Mean Square Error

A measurement of the agreement between theoretical distributions and measured data is the Mean Square Error (MSE)

$$MSE \triangleq \frac{1}{n} \sum_{0}^{n} [F_X^{theoretical}(x) - F_X^{measured}(x)]^2, \tag{8.7}$$

where n is the number of samples, $F_X^{theoretical}(x)$ is given by evaluating the theoretical cumulative distribution function for the measured value x, and $F_X^{measured}(x)$ is defined as the proportion of measured data less than or equal to x.

[2]See B.2.

Chapter 9

Results

An improvement in the agreement with measured data compared to the χ distribution at frequencies between the lowest resonance frequency of the chamber, 58 MHz, and up to 1 GHz is shown for the Bessel K distribution. MSE for the Bessel K distribution, the Compound Exponential distribution with both approximations and the χ distribution are plotted versus frequency in figure A.21 to A.28. In figure A.6 to A.17 is the cdfs plotted. See also table A.1 to see which color that corresponds to which distribution.

9.1 Bessel K

The mean and standard deviation of the measured sample were determined as estimates for μ_s and σ_s respectively. M and B were then estimated from (7.1)-(7.4). M is physically the number of modes, but the estimates for M are normally not integers. Besides this is M surprisingly low, round 0.5 for the lowest frequencies and round 4 for higher frequencies. In [2] it is stated that M is in general large above 300 MHz. In figure A.18 M for E_{tot} are plotted versus frequency. It shows that M increases with frequency but at certain frequencies is M lower than expected, see 570 MHz.

The M-values influence on the Bessel K MSE is examined. M-values are plotted versus MSE, see figure A.19. It show that the MSE-value decrease for increasing M. This agree with the physical interpretation of M as the number of modes in the chamber, if they are very few, the Bessel K model should break down.

For large M, i.e. for high frequencies, the Bessel K and χ distribution should coincide [2].

9.2 Gamma

In figure A.20 is the Gamma distribution for E_{tot} with guessed parameters plotted. At high frequencies is $\eta \approx 0.7$, [2], which with (7.9) gives $\mathcal{M} \approx 23,3$.

9.3 Compound Exponential

For E_{tot} the MSE for the first and second approximation lie close to each other. They are both slightly better than the χ distribution.

The Compound Exponential distribution with the first approximation follow the χ distribution for E_x, E_y and E_z as shown in section 7.3.1.

The second approximation is not applicable at all for E_x, E_y and E_z, see figure A.22.

Since the second approximation is useless for E_x, E_y and E_z, and it is not better than the first approximation for E_{tot}, it is not very interesting. It is not plotted in all MSE figures because that requires a change of the MSE scale which would make the difference between the Bessel K distribution and the χ distribution less clear.

9.4 Correlated samples

We used two stirrers that are stepped independently, and 25×25 stirrer positions to avoid correlated are samples. Are the samples correlated or not? Calculating ρ from (5.1) gives small values for each measurement with two independently rotating stirrers. Uncorrelation is defined as ρ being smaller than, e.g. e^{-1}. Here we get coefficients of order 0.01.

One way to evade the problem with not knowing whether the samples are correlated or not is to do a measurement with obviously correlated samples. Correlated samples is attained with only one stirrer. We did one measurement with only one stirrer, the frequencies were round 570 MHz and the correlation coefficient became 0.6. The difference in correlation coefficient when using one stirrer instead of two stirrers motivate our choice to use two stirrers during all measurements.

Even if the correlation coefficient became larger in the measurement with one stirrer instead of two, the agreement with theories was not affected, see figure A.33 to A.36, this indicates that correlated samples are harmless. Other investigations have shown that data, intentionally repeated to have correlation, do affect the result; data was rejected by a goodness of fit test when they were correlated [6], [13].

9.5 Eigenfrequencies and MSE peaks

First frequencies for which the reflection coefficient is small, and the agreement with the anechoic chamber measurement good, were chosen. Seven frequencies fulfilled these requirements. Those frequencies were chosen to avoid a large reflection coefficient. Then we did a more systematic examination with frequencies chosen at regular intervals.

The first series of measurements does not agree as good as the systematic measurements with theories. In the first measurement series there are more frequencies with large MSE; compare figure A.29 to A.32 with figure A.21 to A.24. An explanation

could be that for eigenfrequencies the reflection is small, because it is easy to find a mode in the chamber. This is good considering reflection, but not so good considering that the modes are very few. It is possible that only one dominant mode is present in the chamber for eigenfrequencies. A dominant mode is difficult to displace by the stirrers. The theories, that is based on a displacement of the modes by the stirrer, fall and give rise to large MSE values.

The idea is that we in the first measurements happened to chose eigenfrequencies when we looked for frequencies with small reflection. This explains the high MSE values at frequencies with low reflection coefficient.

Another explanation for the discrepancy, in agreement between the especially chosen frequencies and the frequencies chosen at regular intervals, is that the frequencies chosen because they have a small reflection coefficient were few, only seven, meanwhile there are several interval measurements that measure about 50 frequencies at a time.

Even during measuring the field for frequencies at regular intervals we get MSE peaks. If the MSE value for the Bessel K or χ distribution exceed 0.1 the frequency is noted in table A.3. Does the theory of a dominant mode at eigenfrequencies also explain high MSE peaks as the one at 570 MHz in figure A.21?

Is the number of modes smaller at frequencies with high MSE values? To examine this we look at the M parameter in the Bessel K distribution, which represent the number of modes. In figure A.18 is it shown that M is much smaller for 570 MHz.

Does the histogram show more outliers at frequencies with MSE peaks? In figure A.5 we have an outlier at 4600 V/m. This is also the value for the peak in figure A.2 which correspond to the same measurement.

The MSE peak for 570 MHz disappear if the field outlier not is taken into account. The M-value, which depend on the variance of the field (see equation (7.1) and (7.3)), increase and hence the MSE will decrease to normal.

The interval round 570 MHz has been further examined to see if the peak can be reproduced. The interval is chosen so that an eigenfrequency statistically exists in the interval. This is done by calculating how close the eigenfrequencies lie at this frequency in an empty chamber, using equation (3.10). The interval is 0.5 MHz wide. Since 50 is the maximum number of frequencies in each measurement the distance between two measured frequencies is 10 kHz. This distance should be small enough to be sure not to miss any eigenfrequency in the interval, if it exist, but figure A.38 does not show any peak that could indicate an eigenfrequency. Not either at 570 MHz in figure A.25 can we see a MSE peak.

In figure A.39 and A.40 we looked for eigenfrequencies round 400 MHz and 580 MHz respectively. Statistically, eigenfrequencies should exist in the chosen intervals. However, there is no indication that eigenfrequencies are tractable by looking at individual frequencies were theories do not hold.

Is it possible to see how the modes move for different stirrer positions? Do any modes seem to be still? In figure A.37 is the field plotted versus frequency for 20 different stirrer positions. No pattern is shown, this is actually good because it indi-

cate that the RC function as it should. It also indicates that the theory of dominant modes to explain individual MSE peaks is wrong.

9.6 Conclusions

The new proposals for distributions functions for the field in undermoded chamber agree well with measured data, especially the Bessel K distribution. Apart from a few frequencies, only about 1 out of 200, the Bessel K distribution has lower MSE than the χ distribution. If you have data from a measurement is it easy to see for which frequencies, if any, the Bessel K distribution breaks down, and eventually ignore the result for these frequencies. The Bessel K distribution can with advantage be used instead of the χ-distribution, even for high frequencies where the distributions coincide.

The Compound Exponential distribution with the first approximation is not very interesting because it is so alike the χ distribution. The second approximation is not interesting at all because it gives large MSE for the component field and is almost identical with the first approximation for the total field.

The good agreement with measured data indicates that it is worth to examine the gamma distribution further.

Acknowledgment

I would like to thank Magnus Höijer at the Swedish Defence Research Agency FOI for introducing me to the subject of reverberation chambers and for his guidance throughout the work. I also express my thanks to Olof Lundén at FOI for all help in performing the measurements and Henrik Shahgholian at the Department of Mathematics at KTH for mathematical and editorial support.

Bibliography

[1] Witters D. and Portnoy S., *Medical Device EMI: FDA Analysis of Incident Reports, and Recent Concerns for Security Systems and Wireless Medical Telemetry*, IEEE EMC Int. Symp., pp. 1298-1291, Montreal, Canada, 2001.

[2] Arnaut L.R., *Limit distributions for imperfect electromagnetic reverberation*, To be published in IEEE Trans. on Trans Electromagn. Compat., vol 45 no. 2 (May 2003).

[3] Taflove A., *Computational electrodynamics The Finite-Difference Time-Domain Method*, Artech House, Boston, 1995.

[4] Höijer M., Andersson A.-M., Bäckström M. and Lundén O., *Three-Dimensional Finite Difference Time Domain Analysis of Reverberation Chambers*, European Symp. on EMC, pp. 263-268, Brugge, Belgium, 2000.

[5] Kostas J. and Boverie B., *Statistical model for a Mode-Stirred Chamber*, IEEE Trans. on Trans Electromagn. Compat., vol.33 no.4, pp. 366-370 (November 1991).

[6] Lundén O., Bäckström M. and Wellander N., *Evaluation of Stirrer Efficiency in FOI Mode-Stirred Reverberation Chambers*, Scientific Report FOI-R-0250–SE, Swedish Defence Research Agency FOI, SE-581 11 Linköping, Sweden, 2001.

[7] Cheng D.K., *Field and Wave Electromagnetics*, Addison-Wesley Publishing Company, Reading Massachusetts, 1989, ISBN 0-201-52820-7.

[8] Blom G., *Sannolikhetsteori och statistik teori med tillämpningar*, Studentlitteratur, 1989, Lund, ISBN 91-44-03594-2.

[9] Arnaut L.R., *Compound Exponential Distribution for Undermoded Reverberation Chambers*, IEEE Transactions on Trans Electromagn. Compat., vol.44 no.3 (August 2002).

[10] Axler S., *Linear Algebra Done Right*, Springer-Verlag, Berlin, 1999, ISBN 0-387-98258-2.

[11] Gut A., *An Intermediate Course in Probability*, Springer-Verlag, Berlin, 1995, ISBN 0-387-94507-5.

[12] Lundén O., Jansson L. and Bäckström M., *Measurements of Stirrer Efficiency in Mode-Stirred Reverberation Chambers*, Technical Report FOA-R–99-01139-612–SE, Swedish Defence Research Agency FOI, SE-581 11 Linköping, Sweden, 1999.

[13] Wellander N., Lundén O. and Bäckström, *The Maximum Value Distribution in an Reverberation Chamber*, in Proc. IEEE Int. symp. on Electromagnetic Compatibility, pp. 751-756, Montréal, Canada, 2001.

[14] Arnaut L.R. and Rochard O.C., *Distributions of Field Magnitude and Energy Density in Undermoded Mode-Tuned Reverberation Chambers*, European Symp. on EMC, Sorrento, Italy, 2002.

[15] FOI, *Elektromagnetiska vapen och skydd*, FOI orienterar om, Nummer 1, Swedish Defence Research Agency FOI, SE-581 11 Linköping, Sweden, 2001.

[16] Anderson H, *Hotbildsstudie. Högeffekt Pulsad Mikrovågsstrålning (HPM)*, Metodrapport FOA-R–99-01244-612–SE, Swedish Defence Research Agency FOI, SE-581 11 Linköping, Sweden, 1999.

[17] Bäckström M., Lundén O. and Kildal P.-S., *Reverberation Chambers for EMC Susceptibility and Emission Analyses*, Review of Radio Science 1999-2000, Chapter 19, Wiley-Interscience, John Wiley & Sons, Inc., New York, 2000.

Appendix A

Figures and tables

Distribution	Color
Bessel K	Red
Chi	Green
Compound Exponential, approx. 1	Cyan
Compound Exponential, approx. 2	Yellow
Gamma	Magenta
Measured	Blue

Table A.1: Distribution functions and MSE values correspond to a color.

Measurement	Frequency [MHz]	Number of frequencies	Number of stirrer positions
1,noise	110 140 215 248 310 375 487	7	25×25
2	350 600 700 800 900 1000	6	25×25
3	50:50:350	7	25×25
4	400:25:550	7	25×25
5	45:5:75	7	25×25
6	80:5:110	7	25×25
7	100:10:600	51	25×25
8	500:10:1000	51	25×25
9	150:1:199	50	25×25
10	400:5:625	50	25×25
11	400:0.01:400.49	50	25×25
12	580:0.01:580.5	51	25×25
13	579.6:0.01:580.1	51	25×25
14	569.8:0.01:570.29	50	25×25
15	569.8:0.01:570.29	50	625
16	270 270 270 270 270	5	25×25

Table A.2: Table of measured frequencies

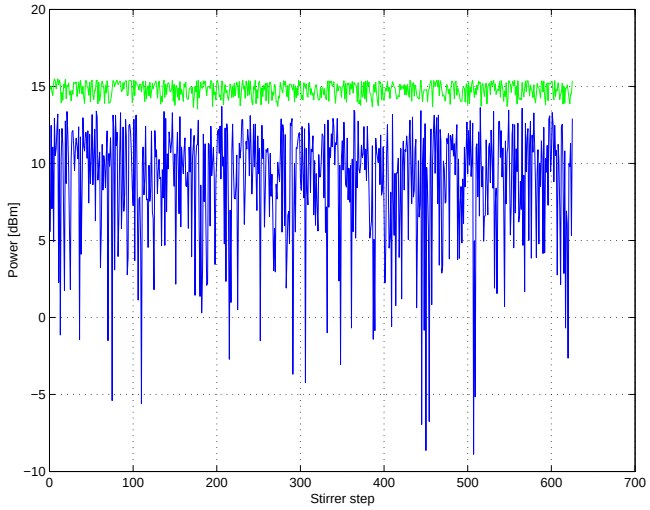

Figure A.1: Transmitted (green) and reflected (red) power at 340 MHz.

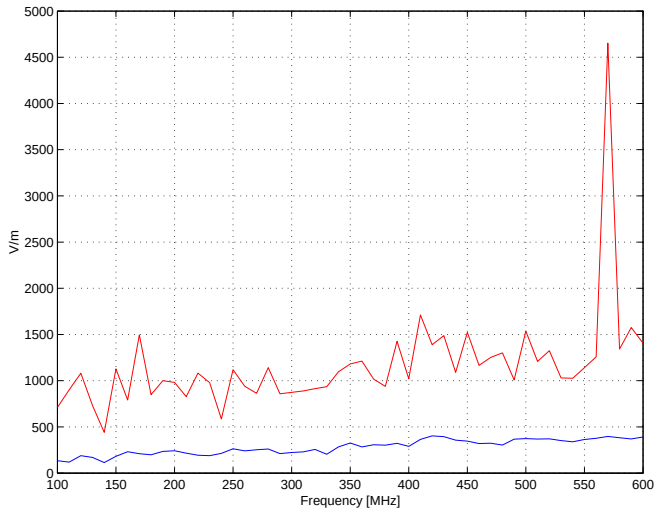

Figure A.2: Mean and maximum for E_{tot}. Outlier at 570 MHz.

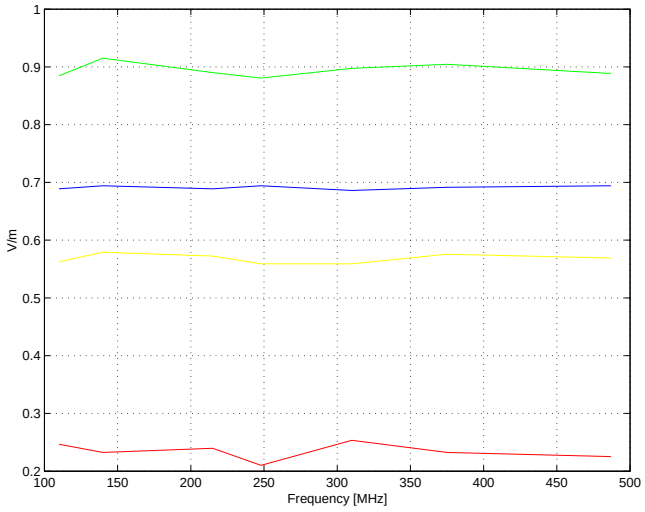

Figure A.3: Maximum noise. Green for E_{tot}, red for E_x, blue for E_y and yellow for E_z

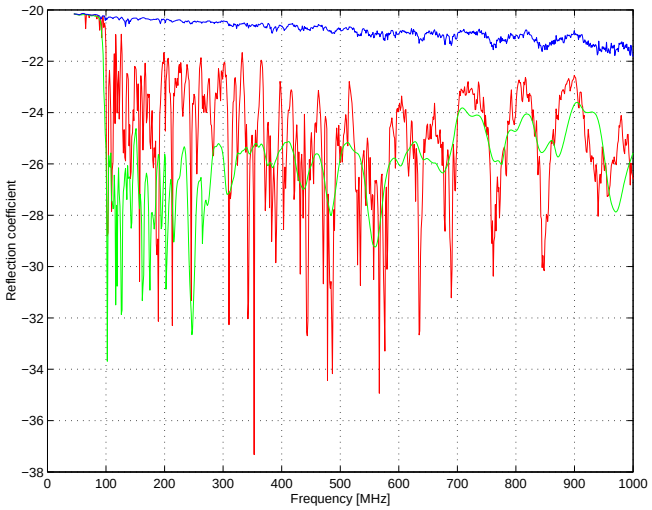

Figure A.4: The mean reflection coefficient over all stirrer positions in the RC is red, the maximum reflection coefficient in the RC is blue and the reflection coefficcient in the AC is green.

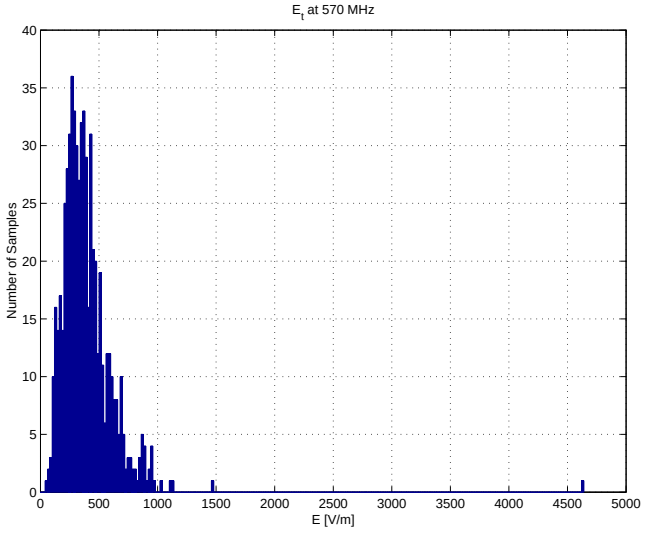

Figure A.5: Histogram for the total field at 570 MHz with an outlier at 4600 V/m

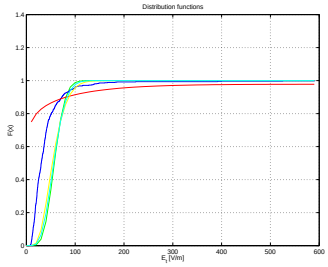

Figure A.6: 50 MHz, E_{tot}

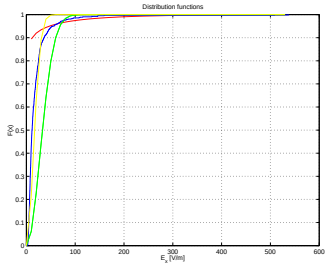

Figure A.7: 50 MHz, E_x

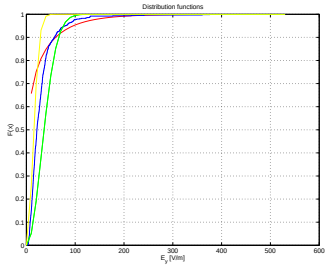

Figure A.8: 50 MHz, E_y

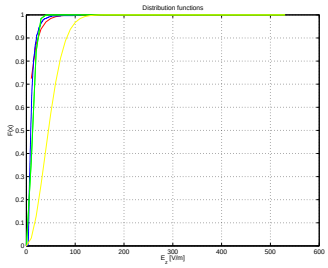

Figure A.9: 50 MHz, E_z

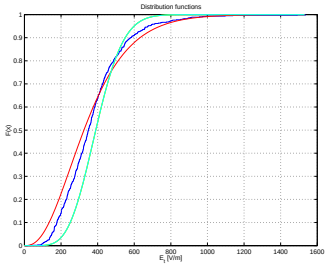

Figure A.10: 500 MHz, E_{tot}

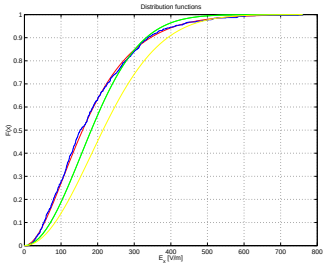

Figure A.11: 500 MHz, E_x

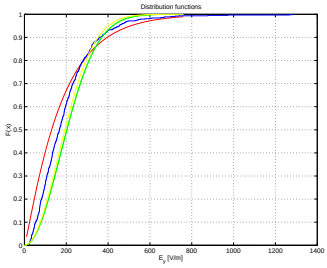

Figure A.12: 500 MHz, E_y

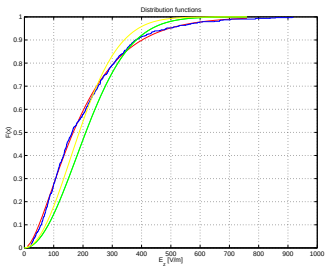

Figure A.13: 500 MHz, E_z

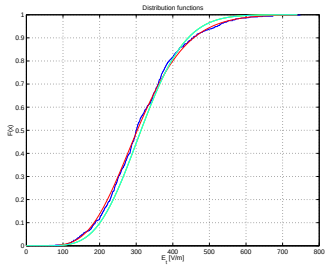

Figure A.14: 1000 MHz, E_{tot}

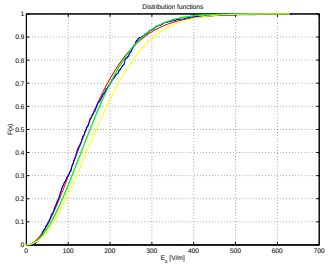

Figure A.15: 1000 MHz, E_x

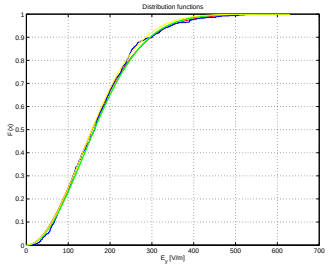

Figure A.16: 1000 MHz, E_y

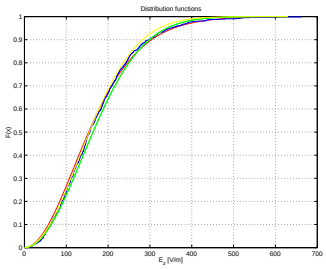

Figure A.17: 1000 MHz, E_z

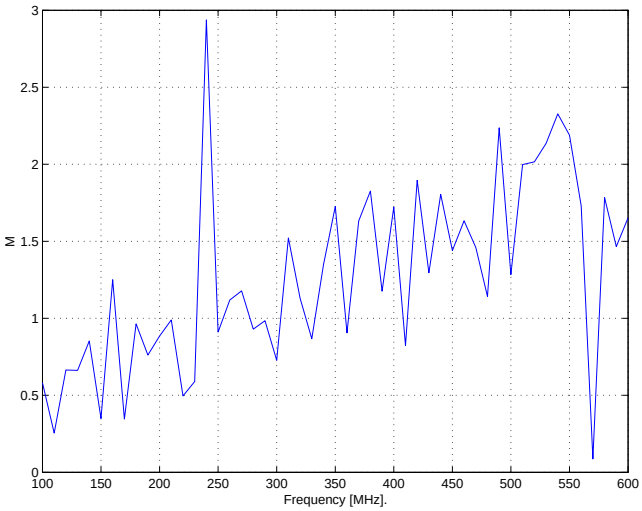

Figure A.18: M for E_{tot} versus frequency

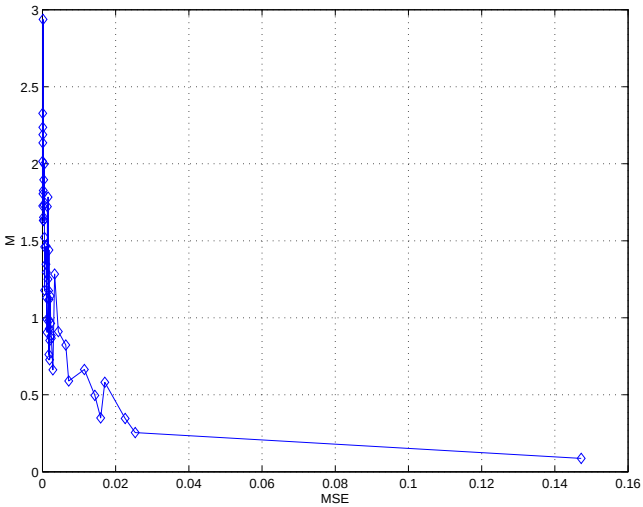

Figure A.19: M for E_{tot} versus MSE

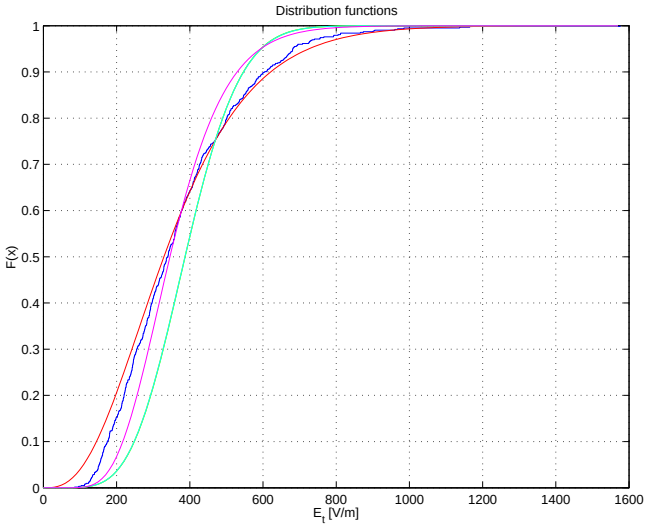

Figure A.20: Distribution functions for E_t at 590 MHz, the Gamma distribution is colored with magenta.

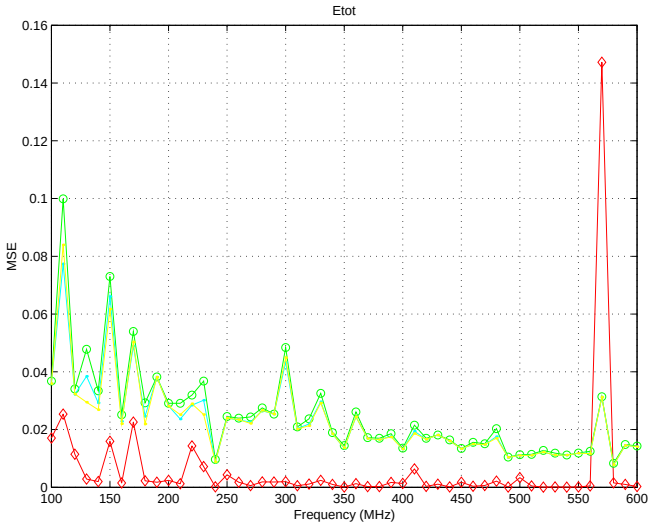

Figure A.21: MSE for E_t

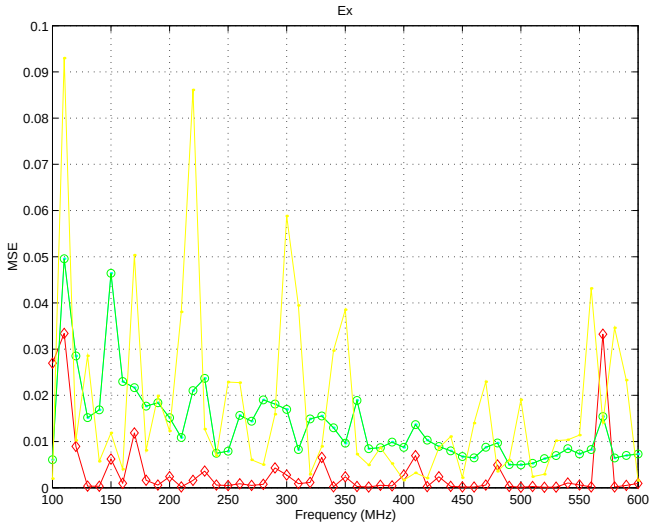

Figure A.22: MSE for E_x

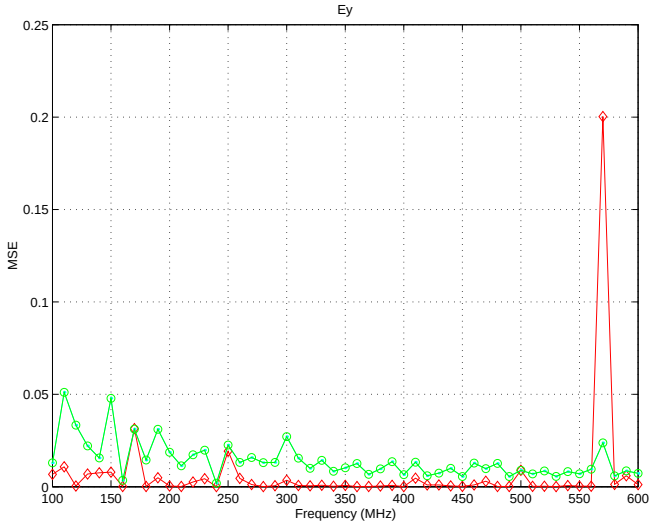

Figure A.23: MSE for E_y

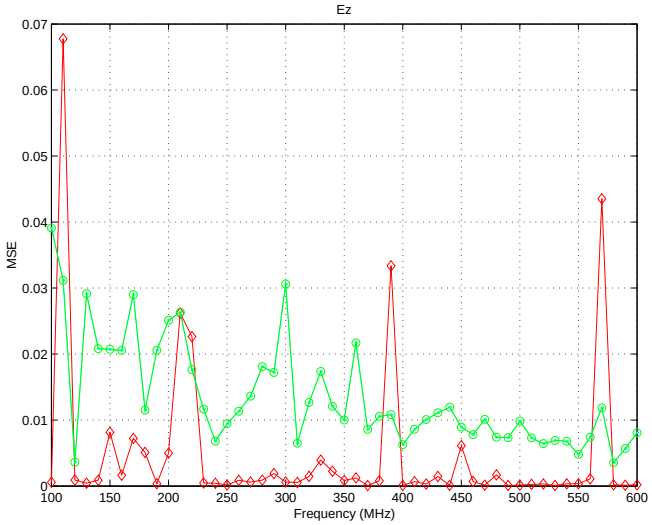

Figure A.24: MSE for E_z

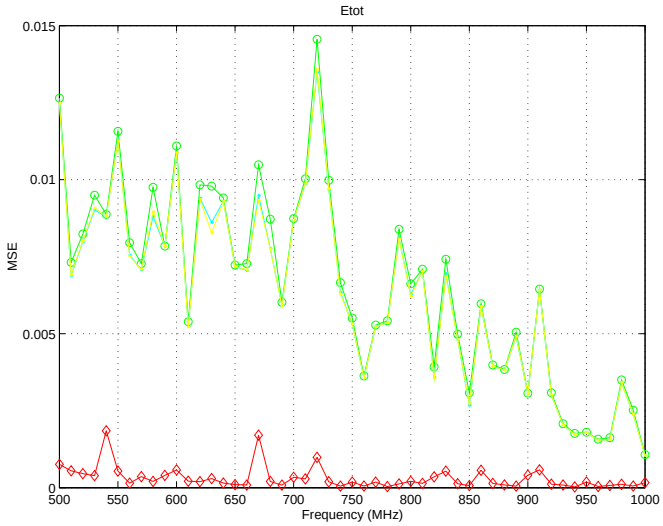

Figure A.25: MSE for E_t

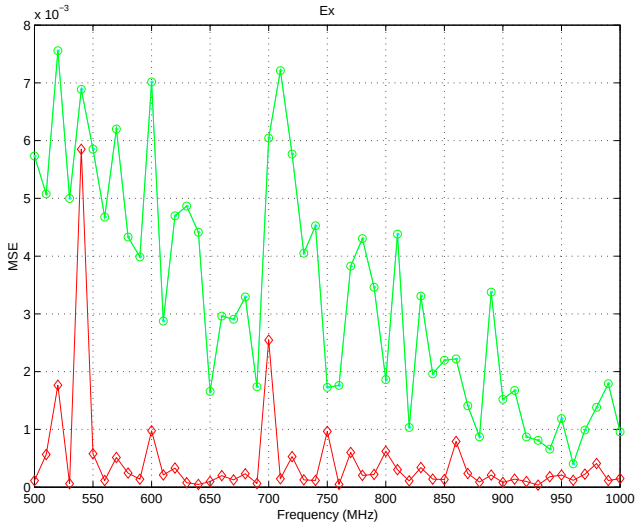

Figure A.26: MSE for E_x

Measurement	E_{tot} [MHz]	E_x [MHz]	E_y [MHz]	E_z [MHz]
1	250	250	250 487	250 487
3	50:50:350	50 150 250 350	100 150 200 300	100:50:300
5	50 70	50 70	70	70
7	570		570	

Table A.3: Table of frequencies that give high MSE.

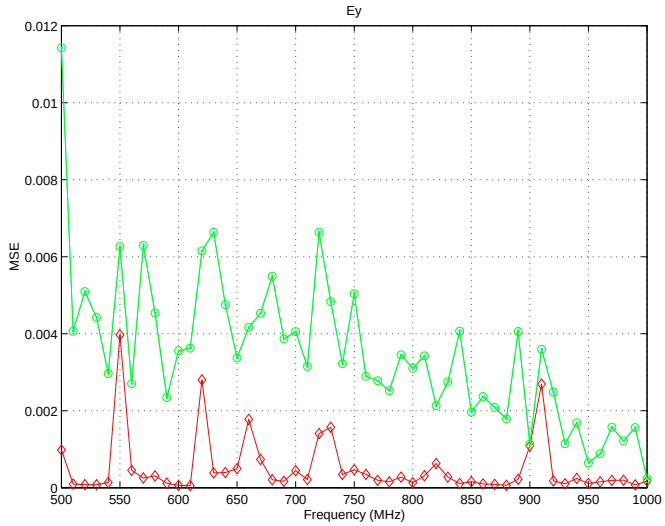

Figure A.27: MSE for E_y

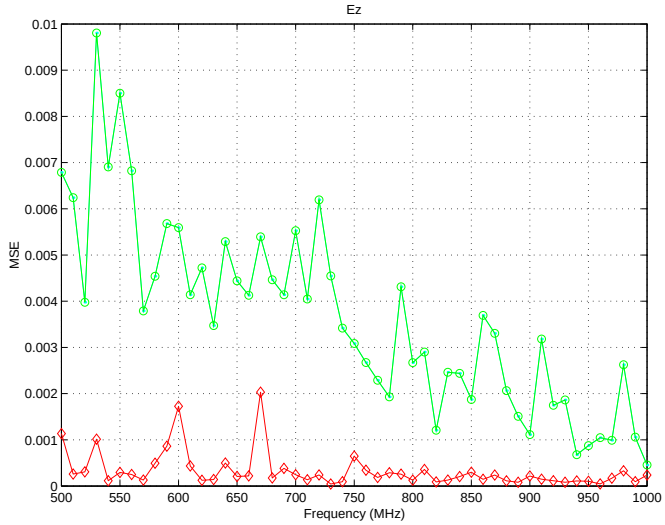

Figure A.28: MSE for E_z

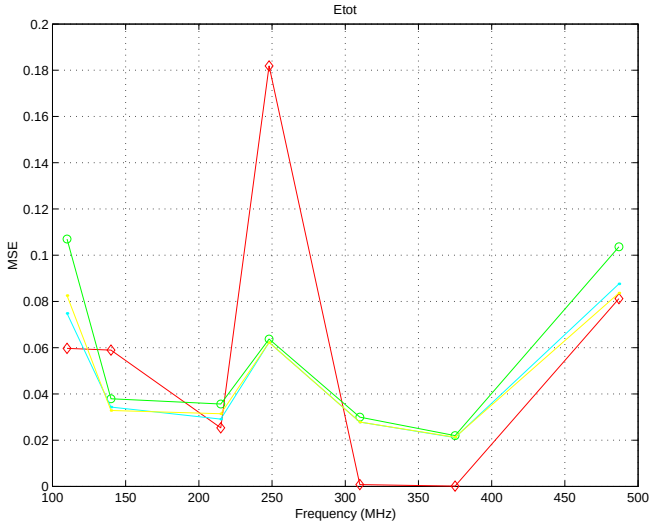

Figure A.29: MSE for E_t, frequencies with low reflection coefficient.

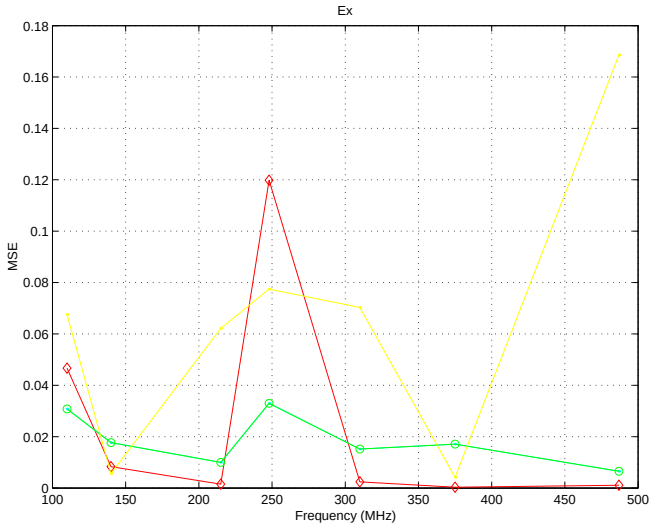

Figure A.30: MSE for E_x, frequencies with low reflection coefficient.

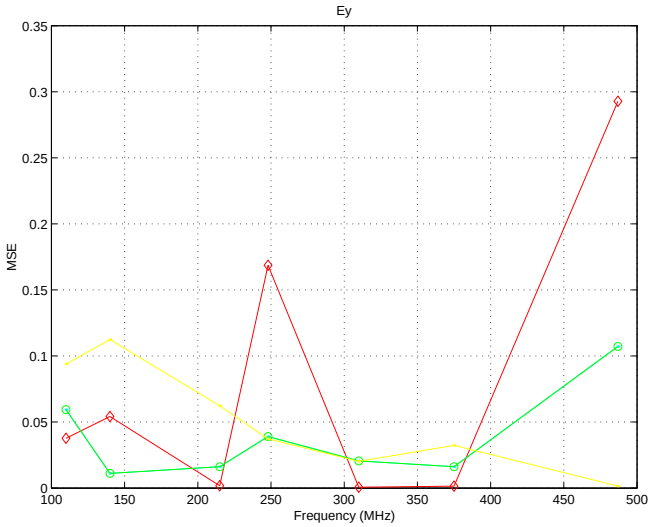

Figure A.31: MSE for E_y, frequencies with low reflection coefficient.

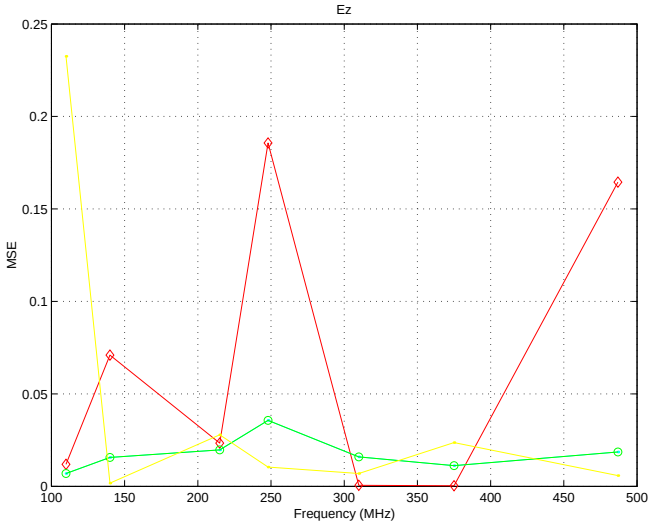

Figure A.32: MSE for E_z, frequencies with low reflection coefficient.

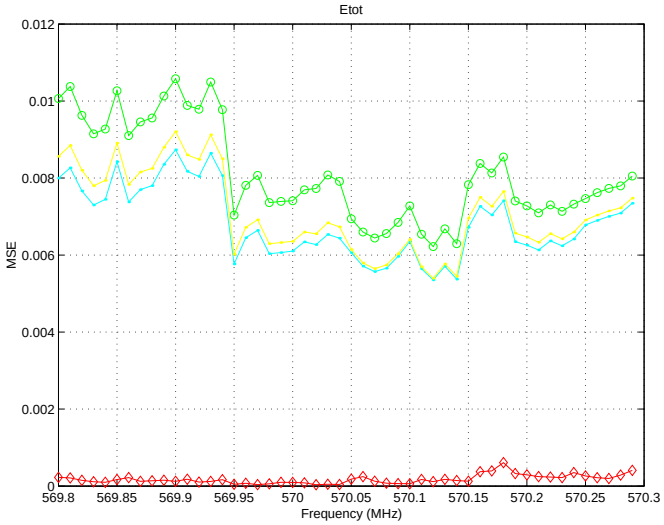

Figure A.33: MSE for E_t, one stirrer

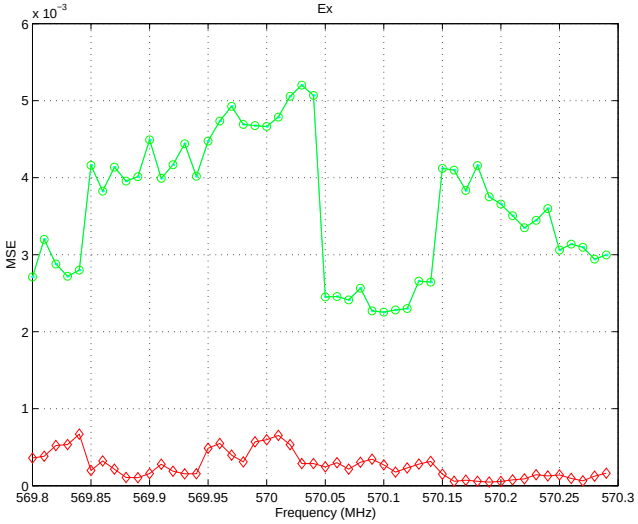

Figure A.34: MSE for E_x, one stirrer

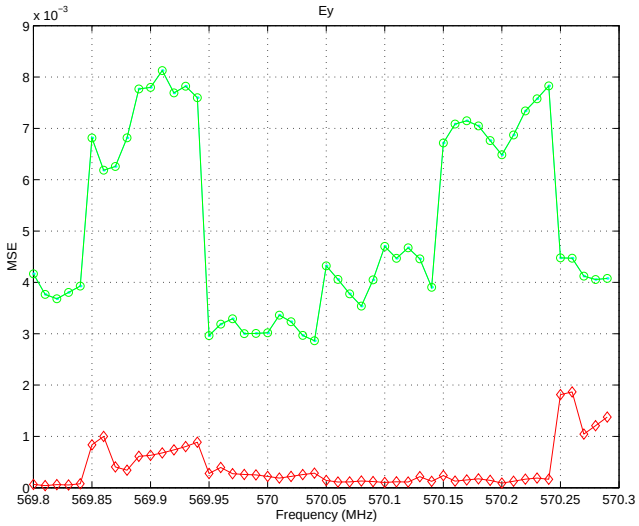

Figure A.35: MSE for E_y, one stirrer

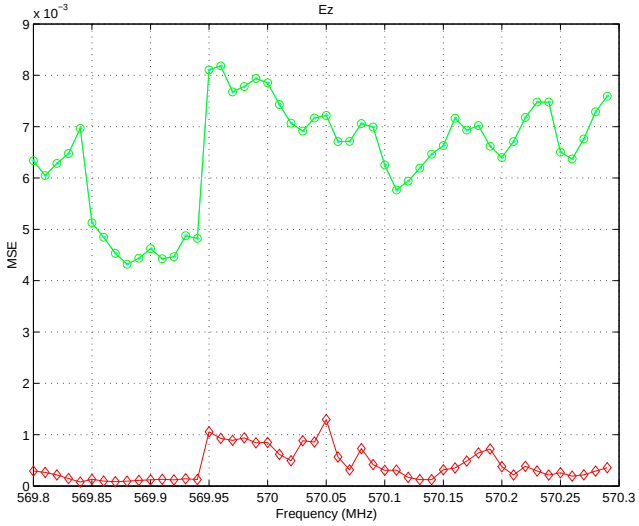

Figure A.36: MSE for E_z, one stirrer

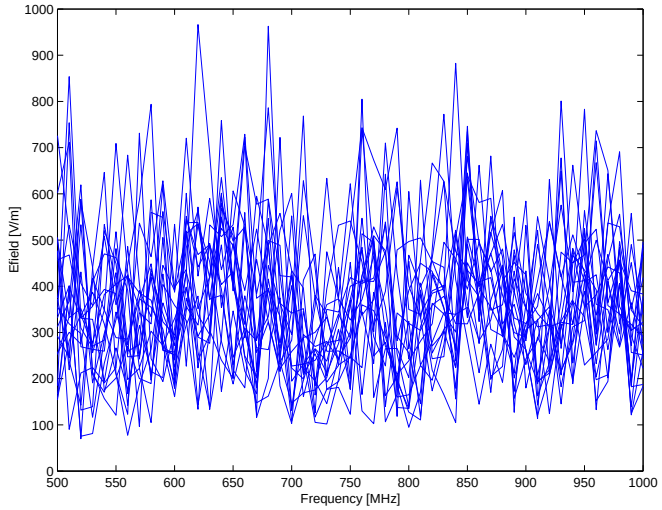

Figure A.37: Efield for 20 stirrer positions vs frequency

Figure A.38: MSE for E_{tot}

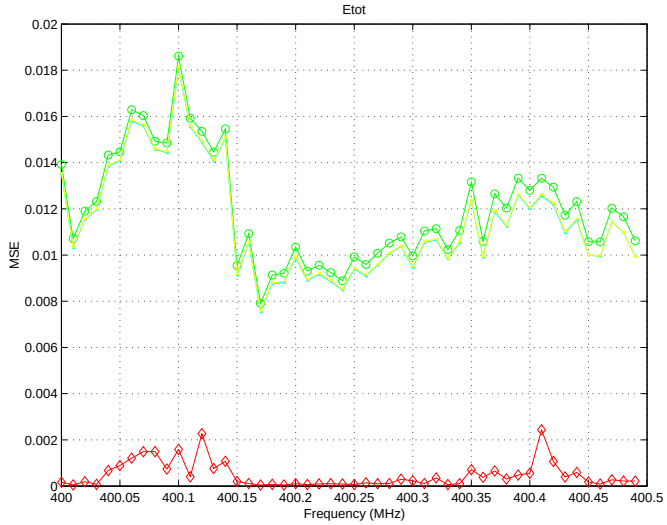

Figure A.39: MSE for E_{tot}

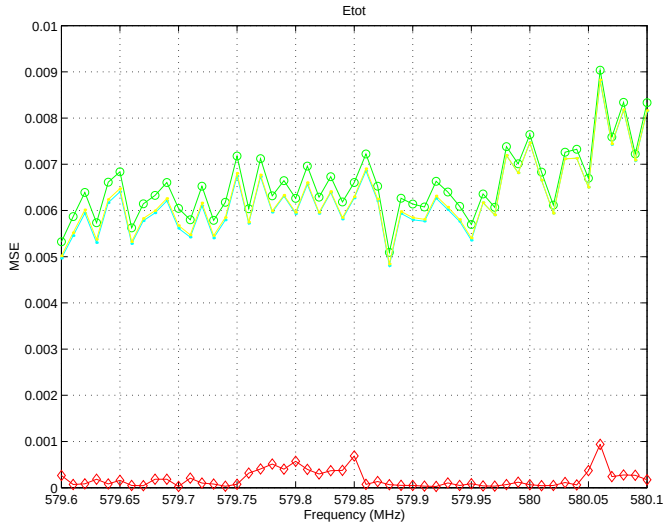

Figure A.40: MSE for E_{tot}

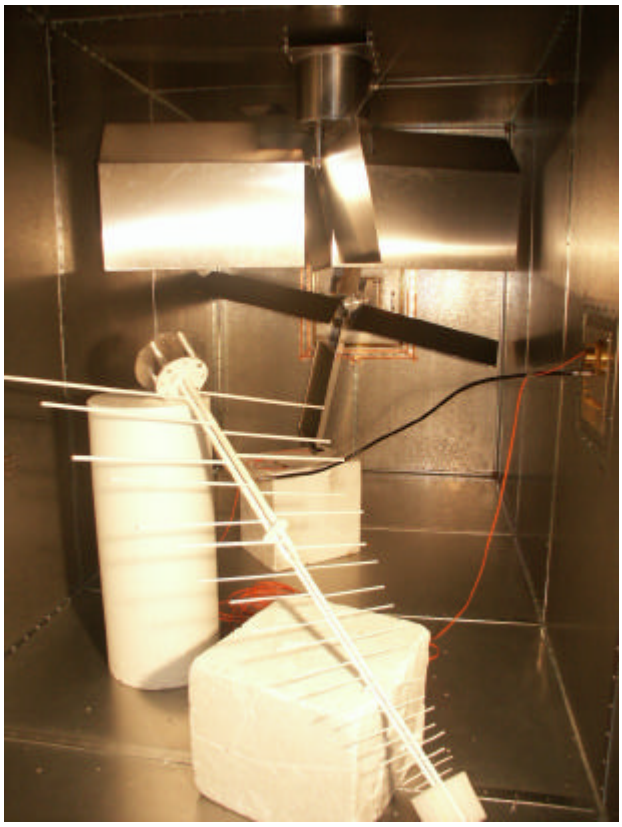

Figure A.41: The reverberation chamber

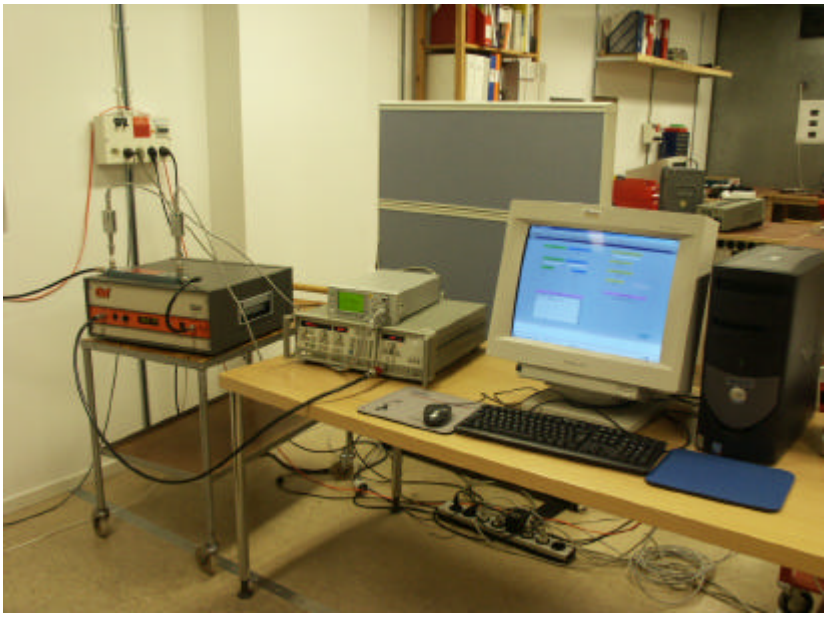

Figure A.42: Amplifier, power meter and PC

Figure A.43: The E-field probe

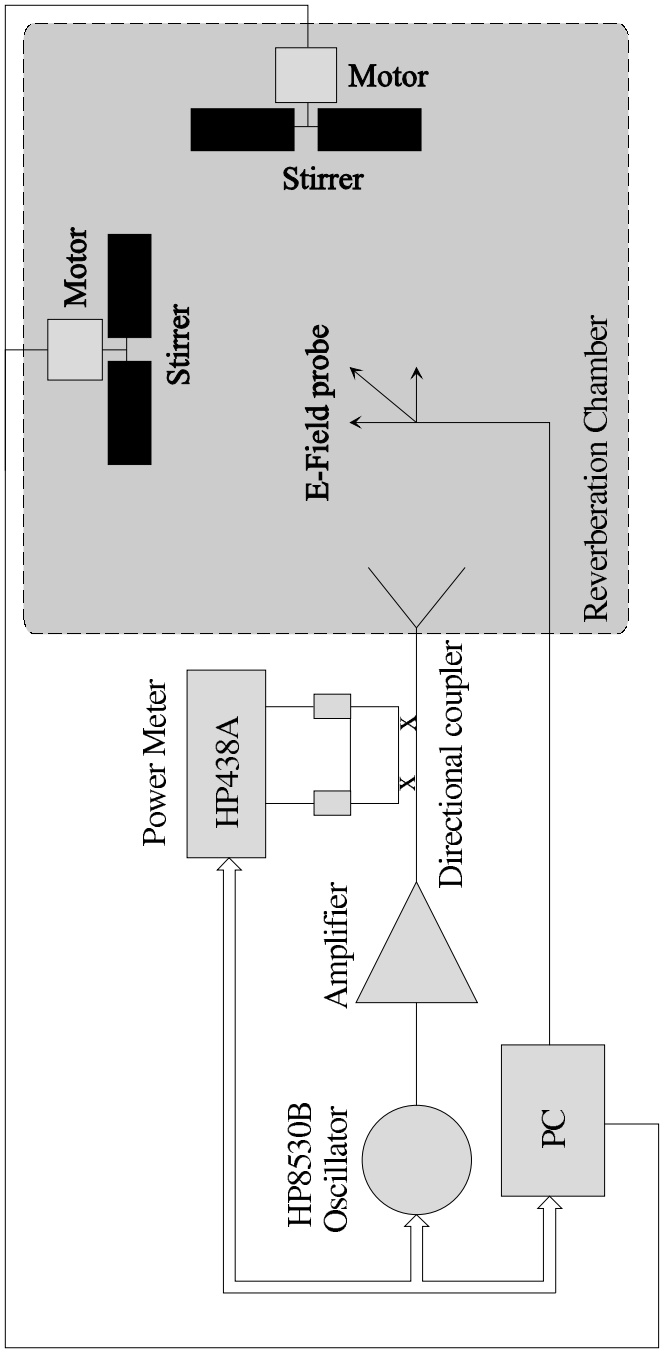
Motor
Stirrer
Motor
Stirrer
E-Field probe
Reverberation Chamber
Power Meter
HP438A
X
X
Directional coupler
Amplifier
HP8530B
Oscillator
PC

Figure A.44:

Appendix B

Explanation of dB and dBm

F is a reinforcement.

$$F_{dB} = 10log_{10}F \tag{B.1}$$

F	F_{dB}
1	0
10	10
$\frac{1}{10}$	-10

P	P_{dBm}
1mW	0dBm
1W	30dBm
1μW	-30dBm

dBm is a unit for power relative to 1mW (Watt).

$$P_{dBm} = 10log_{10}\frac{P}{1mW} \tag{B.2}$$

Appendix C

Reflection in the antenna

To determine the amount of transmitted power reflected back by the antenna, the reflection coefficient S_{11} was measured by the network analyzer.

The reflection coefficient for the antenna was also measured in FOI anechoic chamber for the same frequencies. This result is comparable to the mean of the coefficient over all stirrer positions in the reverberation chamber. See figure A.4.

Averaging across all stirrer position in the RC is closer to the reflection coefficient measured in the AC for higher frequencies.

These data were never used in the results, instead we used data from the power meter.